HEAT AND MASS TRANSFER IN THE VICINITY OF THE VAPOR-GAS FRONT IN A GAS LOADED HEAT PIPE

January 1971

D. K. Edwards
and
B. D. Marcus

Materials Science Department
TRW SYSTEMS GROUP

ABSTRACT

An analysis is presented of axially conducting gas controlled heat pipes leading to a predictive capability for the heat and mass transfer along the heat pipe. In addition, experimental results are presented which verify the analysis, and computational results are presented which show the relative influence of various parameters which affect the system behavior. In particular, it was found that axial heat conduction is of much greater importance than axial mass diffusion in establishing the wall temperature profiles and condenser heat transfer characteristics of gas loaded heat pipes. However, mass diffusion and, consequently, the choice of working fluid and control gas are of considerable importance in establishing the "diffusion freezeout rate" if the potential exists for freezing of vapor which penetrates the gas-blocked portion of the condenser.

It is believed that the analysis and associated computer program are useful tools for designing gas loaded heat pipes.

Introduction

The heat pipe is rapidly becoming a key design element in the solution of a multitude of thermal control and heat transfer problems. In most cases such applications involve conventional heat pipes consisting of a sealed, internally wicked vessel which contains an appropriate quantity of a single working fluid. Such heat pipes are nearly uniform in temperature over their entire surface under most steady-state and transient conditions.

There are several situations, however, where one purposefully introduces a second, non-condensible fluid into the heat pipe so that it will not operate at a uniform temperature. One such situation involves the use of non-condensible gas to effect heat pipe temperature control [1, 2]. Another uses non-condensible gas to aid start-up from a frozen state [3, 4, 5].

Whenever a heat pipe contains a non-condensible gas in addition to its primary working fluid, its ability to transfer heat is altered significantly from that of a conventional heat pipe. During operation of such a heat pipe, vapor flows from the evaporator to the condenser region. As a consequence, any non-condensible gas present in the vapor is swept along and, since it does not condense, accumulates at the condenser end, forming a gas plug (Fig. 1). This gas plug represents a diffusion barrier to the flowing vapor and very nearly "shuts off" that portion of the condenser which it fills. Consequently, by varying the length of this gas plug, one varies the active condenser area and, hence, the heat transfer from the system.

In applying this principle to the design of heat pipes, it has generally been assumed in analytical models that axial conduction can be neglected and that there exists a sharp interface between the vapor and non-condensible gas [1, 2]. This "flat-front" assumption is, however, inconsistent with experimental observations which show that the decrease in vapor concentration and the corresponding increase

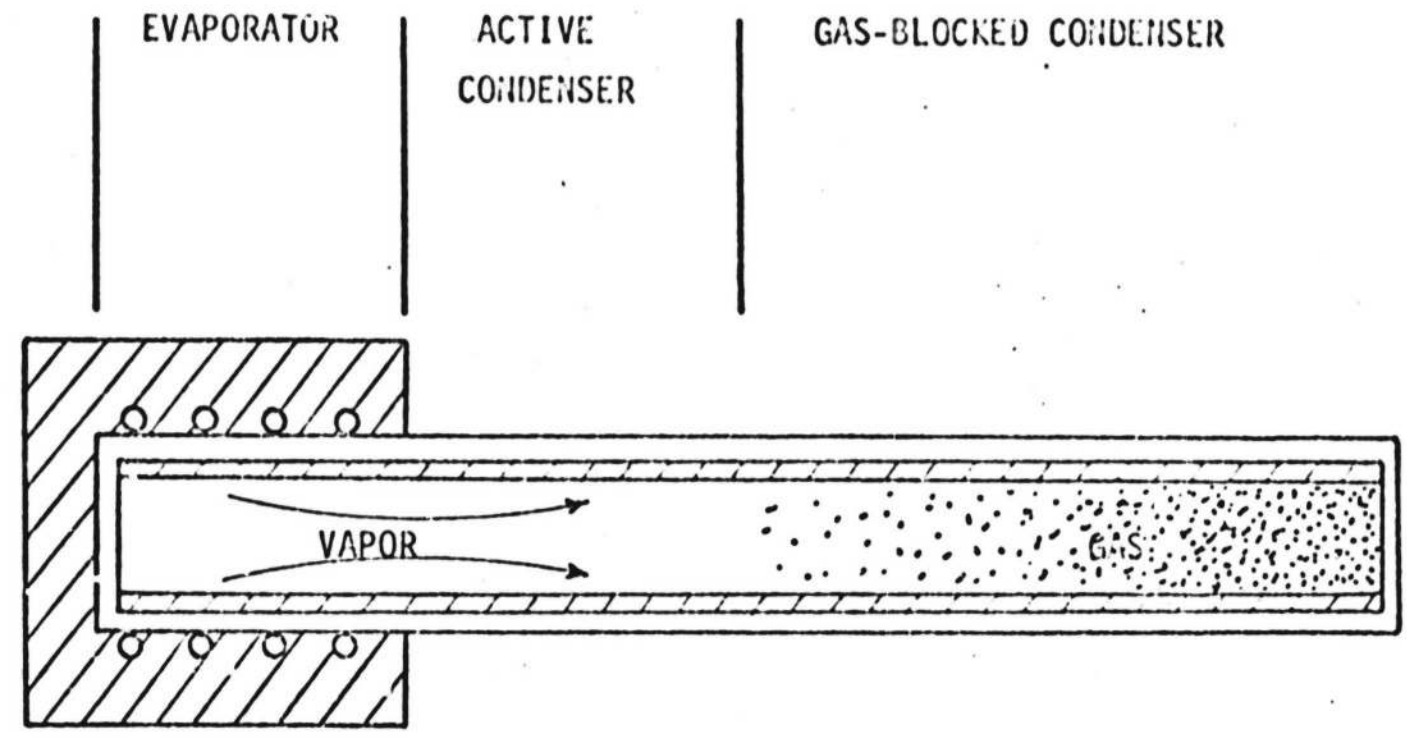

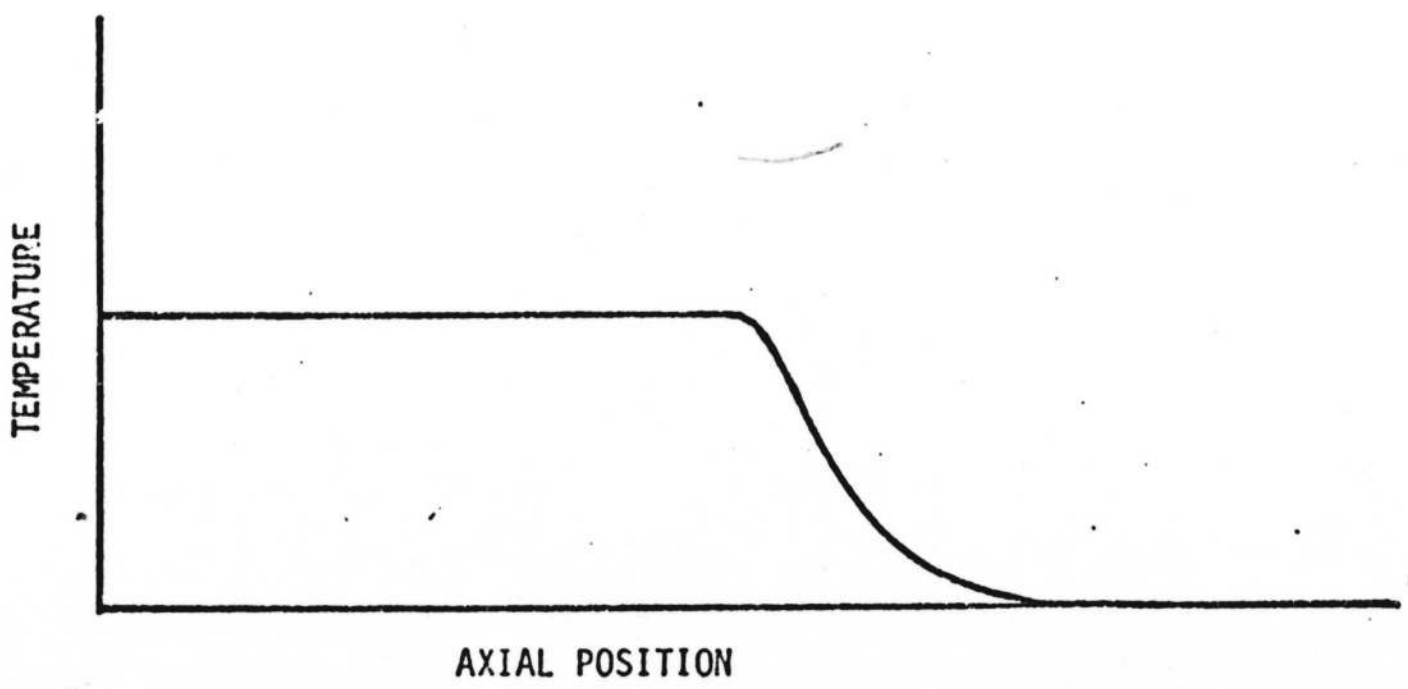

FIGURE 1. Schematic Diagram and Temperature Distribution of a Gas Loaded Heat Pipe.

in gas concentration occur smoothly over an appreciable length of the heat pipe. As a consequence, the flat-front theory does not predict performance very well [2] and is incapable of predicting the rate at which frozen working fluid accumulates when the condenser sink temperature falls below the freezing point.

This paper presents an analysis of axially conducting gas controlled heat pipes, leading to a predictive capability for the heat and mass transfer along the heat pipe. In addition, experimental results are presented which verify the analysis, and computational results are presented which show the relative influence of various parameters which affect the system behavior. In particular, it is shown that axial conductance is of principal importance for low pressure pipes. At high pressures axial diffusion is also an important mode of energy transfer.

Formulation

The condensing section of the pipe is assumed to reject heat by radiation and convection from a fin of perimeter P with an effectiveness η as shown in Figure 2. The net heat loss from a length of condenser dz is thus taken to be

$$d\dot{Q} = \left[\varepsilon\sigma T_w^4 + h(T_w - T_f) - q_{abs}\right] \eta P dz \qquad (1)$$

where ε is total hemispherical emittance, σ the Stefan-Boltzmann constant, T_w the wall temperature, h the convective heat transfer coefficient, if any, T_f the external fluid temperature, and q_{abs} is the power absorbed per unit area from the surrounds, αH in the case of irradiation H onto the condenser surface of absorptance α. For simplicity all parameters are taken to be constants, but a step change is allowed between sections of condenser.

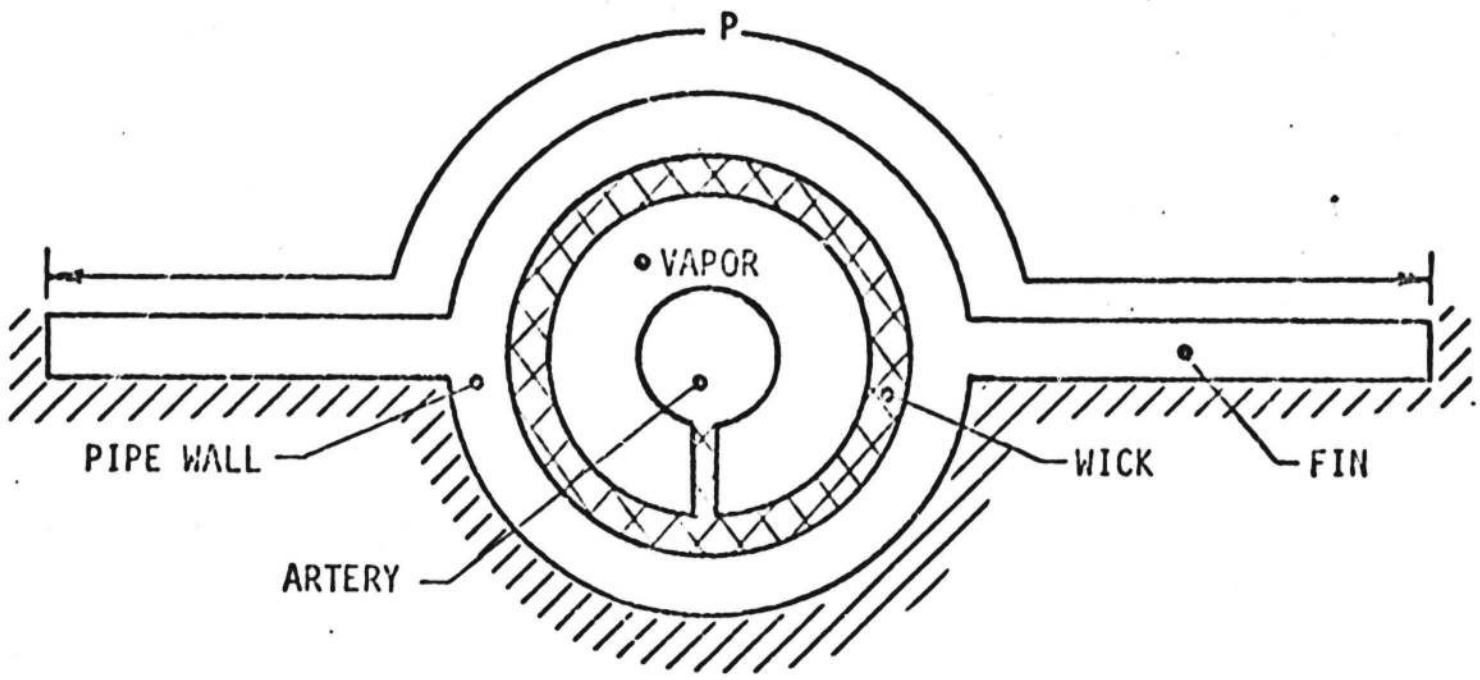

FIGURE 2. Cross-section of Condenser

In the usual heat pipe application the difference between the wick-vapor interface temperature T_i and the condenser wall temperature T_w is small compared to absolute temperature level. For this reason Eq. (1) is written in a linearized form

$$d\dot{Q} = Sdz\ (T_w - T_c) \tag{2}$$

where

$$S(z) = \left[4\varepsilon\sigma T_i^{\,3} + h\right] \eta P \tag{3}$$

and

$$T_c(z) = \frac{3\varepsilon\sigma T_i^{\,4}(z) + q_{abs} + hT_f}{4\varepsilon\sigma T_i^{\,3} + h} \tag{4}$$

We adopt the unusual sign convention that the power $\dot{Q}$ is measured in the negative z direction. Then Fourier's law is written without the usual negative sign. Heat flows into an element of pipe dz long at z+dz and out at z by axial conduction. Heat also flows across the wick by conduction at the rate

$$\frac{2\pi k_e dz}{\ell n \dfrac{D_i+2\delta}{D_i}} (T_i - T_w) = Kdz\ (T_i - T_w) \tag{5}$$

where k_e is the equivalent conductivity of the liquid-filled wick, D_i the inside diameter of the wick, and δ the wick thickness. Equation (5) defines K. The heat balance on an element of condenser is then

$$C\frac{d^2T_w}{dz^2} + K(T_i - T_w) - S(T_w - T_c) = 0 \tag{6}$$

where C is the axial conductivity-area product for the condenser cross-section,

$$C = \sum_{n=1}^{N} k_n A_{c,n} \tag{7}$$

In Eq. (7) k_n is the effective axial conductivity, allowing for slots or other anisotropies, and $A_{c,n}$ the cross-sectional area of the nth element in the pipe. These elements may include the pipe wall, the wick and any arteries, and the fin wall, as shown in Fig. 2. Even if the wick artery is not in intimate thermal contact with the condenser wall, its axial conductance is included in Eq. (7), because the temperature gradient in it tends to follow dT_i/dz which in turn tends to follow dT_w/dz, when K is large compared to S.

The wick interface temperature T_i is the saturation temperature for the partial pressure of the vapor above the interface, since the net condensation rate is far from the absolute rate of condensation (kinetic limit). Other simplifying assumptions introduced, which are reasonable for most applications, are negligible vapor side pressure loss and a simple vapor pressure law derived from the Clausius-Clapeyron relation. The mole fraction of the non-condensible at the interface x_i and the interface temperature T_i are then related in the following way

$$x_i = 1 - \exp\left[-(h_{fg}/RT_{ev})(T_{ev}/T_i - 1)\right] \tag{8a}$$

$$T_i = \frac{T_{ev}}{1 + \frac{RT_{ev}}{h_{fg}} \ell n \frac{1}{1-x_i}} = \frac{T_{ev}}{1 + \frac{T_{ev}}{T_o} \ell n \frac{1}{1-x_i}} \tag{8b}$$

Conservation of non-condensible gas requires that the diffusion plus convection in the tube sum to zero,

$$-c\mathscr{D}\frac{dx_s}{dz} - cVx_b = 0 \tag{9}$$

where c is the molar concentration, $\mathscr{D}$ the diffusion coefficient for the non-condensible diffusing in the vapor, x_s the spatial or area-weighted average mole fraction, V the mole average velocity, and x_b the bulk (area-velocity weighted) average. At least in the region

of the condenser which is gas-controlled, the radial velocity rates will be sufficiently low so that the bulk, spatial, and wall values of mole fraction of non-condensible will be nearly the same. This assumption is made for the entire condenser so that the subscripts i, s, and b on x will be dropped in what follows.

To obtain an equation having the grouping $\dot{m} = cVA_cM$, the condensible flow rate, Eq. (9) is multiplied by A_cM, where M is the molecular weight of the condensible working fluid. In addition, the dependent variable is transformed from mole fraction x to ϕ by introducing

$$\phi = \ell n \frac{1}{x}, \quad x = e^{-\phi} \tag{10}$$

Equation (9) then becomes

$$A_cM\mathscr{P}\frac{d\phi}{dz} + \dot{m} = 0 \tag{11}$$

Conservation of mass shows that increase in mass flow rate with distance from the end of the condenser is equal to the condensation rate which in turn is equal to the product of wick conductance and temperature differerce across the wick divided by the latent heat of vaporization or sublimation.

$$\frac{d\dot{m}}{dz} = K(T_i - T_w)/h_{fg} \tag{12}$$

Equations (6), (11) and (12) form a set of three simultaneous differential equations in three unknowns: T_w, ϕ, and $\dot{m}$. The temperature T_i is related to ϕ through the highly nonlinear relations, Eqs. (10) and (8). The coefficient S defined by Eq. (3) is also nonlinear. An explicit energy equation for the liquid or vapor is not written, because subcooling of liquid in tne wick and superheating of the vapor in the pipe are not considered to be key physical phenomena, and are neglected in the present treatment. Equations (12) and (6) will give an entirely correct energy balance

when x_i, x_s, and x_b are identical, the wick resistance small, and no freezing occurs.

A boundary condition on (6), (11), and (12) is taken to be

$$\dot{m} = 0 \text{ at } z = 0 \tag{13}$$

In addition, either one of two conditions may be prescribed: a total heat rate rejected

$$\dot{Q} = \int_0^L S(T_w - T_c)dz \tag{14a}$$

or a total number of moles of non-condensible present

$$\mathcal{M} = A_c \int_0^L \left[P_i(T_i(z))/R_u T_i\right] dz \tag{14b}$$

In computing $\mathcal{M}$ a more accurate vapor pressure law than Eq. (8) must be used. An exponential of a polynomial in the reciprocal of T_i is thought best.

Strictly speaking, since Eq. (6) is second order, two more conditions must be specified, such as a zero CdT_w/dz at $z = 0$ and $z = L$. However, an approximation is made that the first and second derivatives of T_w with respect to z are equal to those of T_i. As is shown in the Appendix this approximation reduces the set of equations to two first order ones so that Eq. (13) and (14) are sufficient. The condition on CdT_w/dz is met at $z = 0$, and at $z = L$ it is met in practical effect when the evaporator is purged of gas. The approximation regarding the derivatives of T_w and T_i is, of course, exact when the wick resistance is zero.

A review of the features of the analysis and assumptions made are as follows:

1. Radiation and convection from a finned pipe is considered. Absorbed radiation from the surrounds is included.

Provision for a step change in condenser properties and ambient conditions is made.

2. The condenser wall temperature T_w is assumed close to the wick interface temperature T_i. The first and second derivatives of T_w and T_i with respect to z are assumed equal, respectively. In essence high wick conductance is assumed.
3. Axial conduction of heat in the pipe wall and fin and one-dimensional axial diffusion of the condensible species, which carries latent heat, is accounted for.
4. Vapor pressure drop in the pipe is neglected. In calculating the shape of the wall temperature and wick temperature distributions, an approximate vapor pressure law derived from Clausius-Clapeyron is used. But in calculating the pressure in the pipe and the amount of non-condensible present a more accurate expression is used.
5. The condition of zero wall temperature gradient is met at z = 0. Either the total number of moles of non-condensible present in the pipe or the total heat rejected by the pipe is specified.

Numerical Solution

The appendix shows how Eqs. (6), (11), and (12) are reduced by virtue of assumption 2 above to a set of two simultaneous first order differential equations in ϕ and V*, a dimensionless velocity or $\dot{m}$. An initial value T_i at z = 0 is used to fix $\phi(0)$, and a fourth-order Runge-Kutta routine is used to solve for $\phi(z)$ and V*(z). Either the amount of gas in the pipe or the value of $\dot{Q}$ obtained at length L is then compared to the required value, and $\phi(0)$ is adjusted. This procedure is repeated until the calculated value of $\dot{m}$ or $\dot{Q}$ agrees within one-tenth of one percent with the specified value.

The following input information is required for the numerical solution:

Fluid Characteristics:

Vapor pressure law constants, molecular weight of condensible, binary mass diffusivity of non-condensible into condensible, temperature exponent of diffusivity and latent heat of vaporization.

Vapor Flow, Pipe and Wick Characteristics:

Outside diameter, wall thickness and thermal conductivity of pipe; thickness and effective thermal conductivity of wick; diameter of internal artery, reservoir or reservoir feed tube, if any.

Condenser Characteristics for Each of Two Condenser Sections:

Perimeter, length, effectiveness, heat transfer coefficients, emissivity, thickness and effective axial conductivity of the fin; ambient fluid temperature and power per unit area absorbed on the heat transfer surface.

Operating Conditions:

(a) Evaporator temperature and total heat dissipated, or

(b) Evaporator temperature and moles of gas present in the pipe (in this case a nominal estimate of $\dot{Q}$ ($\dot{Q}_{nominal}$) must be input because it is used for convenience in making dimensionless the equations shown in the Appendix).

The program output consists of profiles of x_i, T_i, T_w, $m(Z)$, $\dot{m}$ and $\dot{Q}(z)$ versus z. In addition, the missing value of $m(L)$ for case (a) above or a correct value of $\dot{Q}(L)$ for case (b) is obtained.

Comparison with Experiment

A series of measurements were made with a laboratory gas-loaded heat pipe to provide a basis for testing the predictive capability of the gas front computer program. The design details of the heat pipe are presented in Figure 3 and Table 1.

The heat pipe was instrumented with 24 chromel-alumel thermocouples, 23 on the outside wall and one within the vapor core in the evaporator. In addition, a strain gage pressure transducer was attached to the fill tube. Heat input to the 12 inch evaporator was supplied with glass-insulated Nichrome heating wire close-would around the pipe wall. The evaporator and adiabatic sections were insulated with 2 inches of polyurethane foam. Heat transfer from the condenser was by radiation and natural convection to ambient.

Additional instrumentation included an ammeter and voltmeter for power measurements, a multipoint recorder and a hand balanced potentiometer for temperature measurements, a digital voltmeter and transducer power supply for pressure measurements, and a precision thermometer and barometer for measuring ambient conditions.

The experimental procedure involved simply setting a fixed power input to the heater, allowing the system to equilibrate (using the multipoint recorder as an indicator), and then recording the appropriate data (using the potentiometer for accurate temperature measurements). Five runs were made in total, such that the vapor-gas interface traversed the entire condenser.

The non-condensible gas inventory was determined using the pressure transducer attached to the fill tube. The procedure was to turn off the power to the heaters and allow at least twelve hours for the pipe to equilibrate. This rather lengthy equilibration period was required for the vapor and gas to thoroughly diffuse yielding a uniform mixture. The internal total pressure was then measured. The partial pressure

TABLE I

Heat Pipe Design Details

Working Fluid:	Water	
Inert Gas:	Air (2.67×10^{-6} ±5% lb-moles)	
Pipe:	Material:	Stainless Steel
	Outside Diameter:	0.565 in.
	Wall Thickness:	0.036 in.
	Overall Length:	54.75 in.
	Condenser Length:	30.25 in.
	Evaporator Heat Input Length:	12.5 in.
	Adiabatic Section Length:	12.0 in.
Wick Structure:		
	Material:	200 mesh stainless steel screen
	Description:	Concentric annulus artery (0.015 in. gap width) with two wraps of screen held in place by a spring.

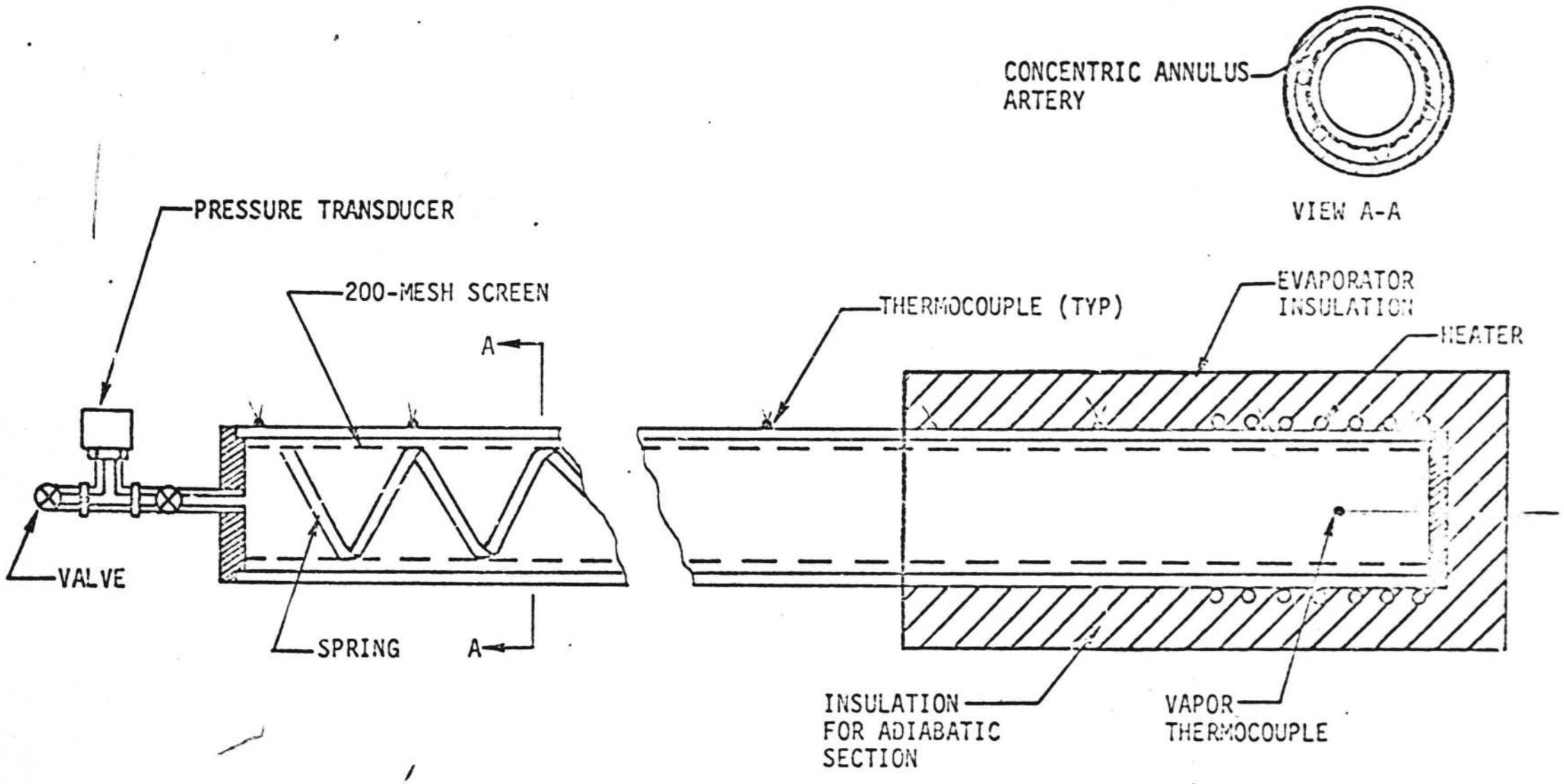

FIGURE 3. Schematic Diagram of Experimental Heat Pipe.

of gas was determined by subtracting the vapor pressure of water at measured ambient temperature from the total pressure as measured by the transducer. The molar inventory of gas was then calculated from the perfect gas law since the total void volume of the pipe and the gas temperature were also known. Such measurements were made at the beginning of the test program, midway through it and at the end. All measurements yielded the same gas inventory indicating that no leakage or gas generation occurred during the test program.

The gas-front computer program was then utilized to obtain performance predictions for each of the test runs. The required input data for the program were listed earlier. All but one of the required inputs are either known properties of the materials or directly measured quantities. The exception is the coefficient of heat transfer - h. Since the predicted heat dissipation for a given temperature distribution is quite sensitive to the assumed value of h, this value was determined for each test run by using Newton's cooling law, $q = h\Delta T$, in conjunction with the measured power and temperature distribution. The calculated values of h represent both radiative and natural convection heat transfer. They are of appropriate magnitude for such a heat transfer mode.

Figure 4 presents both the measured and predicted temperature profiles. As is apparent, the gas front program predicts the position of the gas front quite well. This is particularly true in view of the sensitivity of the system to gas inventory and evaporator temperature. The shaded band around one curve on Fig. 4 represents the predicted front positions for a $\pm 5\%$ variation in gas inventory. This is about the limit of accuracy estimated for this measurement. The effect of a $\pm 2°F$ measurement error in evaporator temperature is shown as a shaded band on a second curve. Again, this represents the limit of accuracy estimated for absolute temperature measurements with the system used.

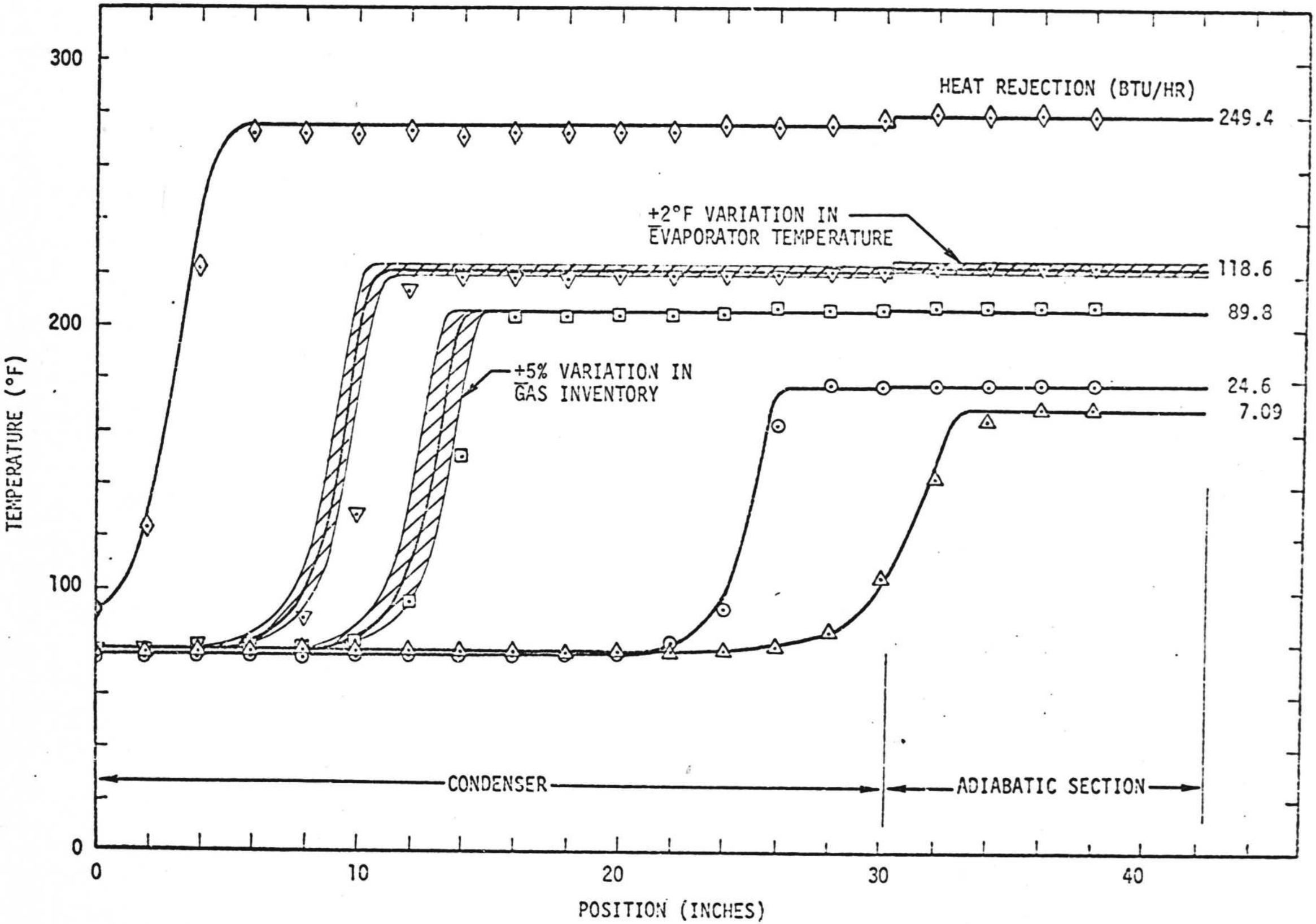

FIGURE 4. Comparison of Measured and Predicted Temperature Profiles for a Gas Loaded Heat Pipe with 12 Inch Adiabatic Section.

The program also does a credible job in predicting the shape of the temperature profile, particularly at the low temperature end. At the high end, the predicted profile rises somewhat more steeply than the measured data. This is due to the approximate method used to account for the radial wick resistance. The analysis allows a somewhat higher condensation rate in this region then actually occurs, leading to a slightly sharper gas front.

Also of interest is the ability of the analysis and computer program to predict the heat rejection vs. evaporator temperature characteristic of the heat pipe. This characteristic describes the steady-state performance of gas loaded heat pipes from a system design point of view. Figure 5 shows the comparison between measured data and the computer predictions. Very good agreement is evidenced between measured and predicted results.

Parametric Study of Gas Front Behavior

With the analysis and computer program experimentally verified, a series of computations were performed to examine the influence of pertinent variables on the nature of the vapor-gas front. Several of the most important results, showing the influence of working fluid, axial wall conductivity and operating (evaporator) temperature are presented here.

A single geometry was used for all calculations so as to isolate the effect of the variable under study. This consisted of a five foot tubular condenser section which was assumed to radiate heat from its surface to an arbitrary heat sink.

The parameters defining the cases studied are presented in Table II. All are self-explanatory except for the "Nominal Gas Length." An input option in the computer program allows one to specify the gas inventory either as the number of moles present or the length of

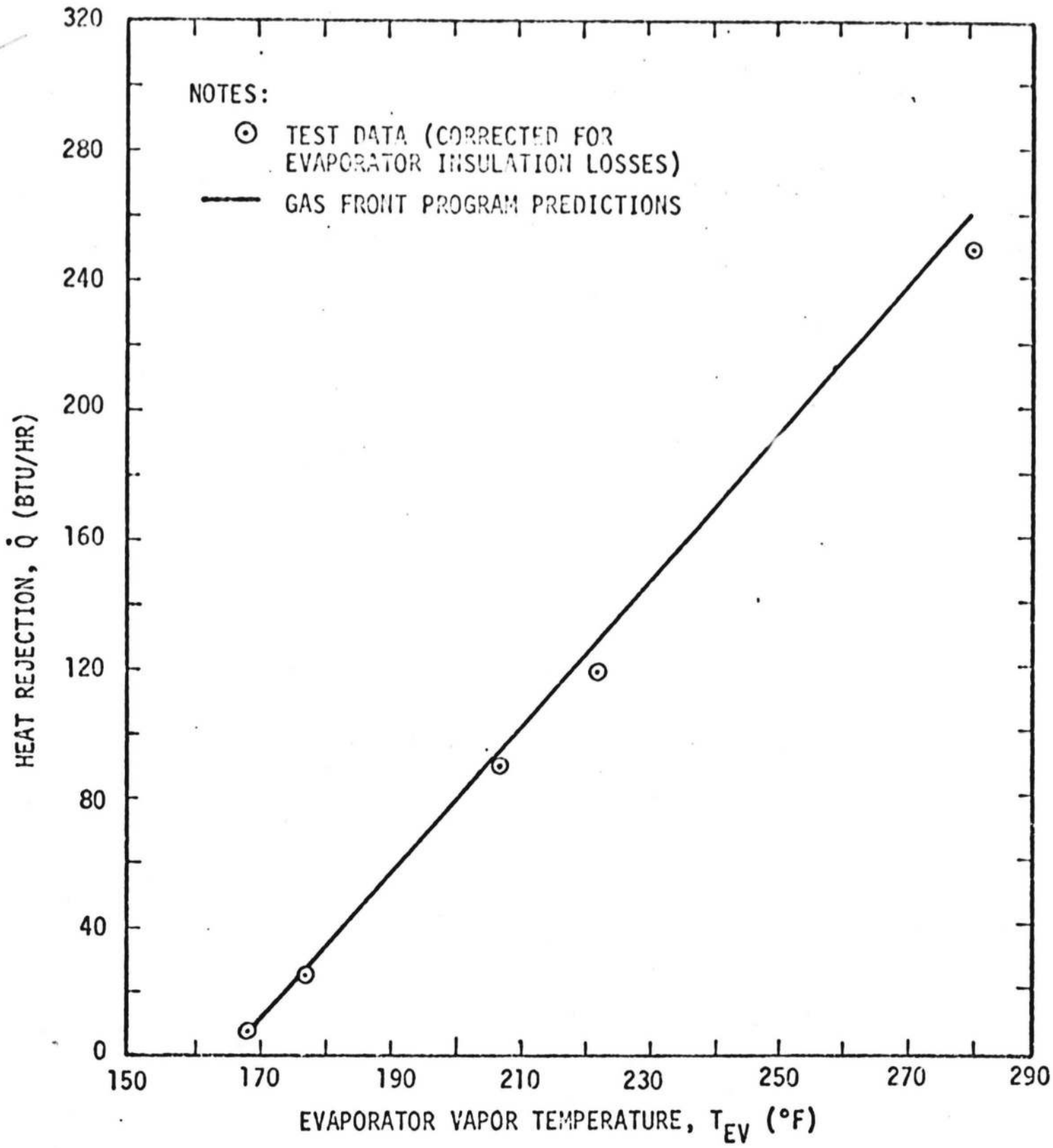

FIGURE 5. Comparison of Predicted and Observed Heat Transfer Rates as a Function of Heat Pipe Evaporator Temperature.

TABLE II

Summary of Cases Studied

Common Variables:

Condenser length	5 feet
Outside diameter	0.5 inches
Wall thickness	0.022 inches
Wick thickness	0.020 inches
Surface emissivity	0.8
Non-condensible gas	nitrogen
Nominal gas length	2.5 feet

Variable Matrix:

Run	Fluid	Material	Evaporator Temp. (°R)	Effective Sink Temp (°R)
1	Methanol	Titanium	550	350
2	Methanol	Stainless Steel	550	350
3	Methanol	Nickel	550	350
4	Methanol	Aluminum	550	350
5	Ammonia	Titanium	550	300
6	Ammonia	Stainless Steel	550	300
7	Ammonia	Nickel	550	300
8	Ammonia	Aluminum	550	300
9	Ammonia	Stainless Steel	550	350
10	Water	Stainless Steel	550	350
11	Ammonia	Stainless Steel	500	300
12	Ammonia	Stainless Steel	450	300
13	Methanol	Stainless Steel	550	300
14	Methanol	Stainless Steel	500	300
15	Methanol	Stainless Steel	450	300

condenser which the gas would occupy based on flat front theory. Using the latter option it was possible to position the fronts approximately midway up the condenser for all cases without tedious calculation of appropriate molar inventories. This permitted a clear comparison of the profiles when comparing different fluids or operating temperatures (and pressures).

Effect of Wall Conductivity:

It was expected that axial conduction in the pipe wall and radiator fins (if any) would play a substantial role in defining the vapor-gas interface. To examine the magnitude of this effect, calculations were performed for titanium, stainless steel, nickel and aluminum heat pipes with methanol and ammonia as the working fluids.*

The calculated temperature profiles along the condenser for methanol are shown on Fig. 6. One clearly sees that wall conductance tends to spread the front over the condenser, and that this can be a very large effect with high conductivity materials like aluminum. Diffuse vapor-gas fronts are undesirable in gas-controlled heat pipes. They tend to decrease control sensitivity [2].

The calculations also yielded the heat transfer from that portion of the condenser which is downstream of the point at which T_i has risen 99% of the way from the sink temperature to the evaporator temperature. This transfer represents the minimum power required to keep the gas blocked zone from entering the evaporator (or adiabatic section if there is one) to any appreciable extent. The results, which are presented in Table III, clearly show that this value is also sensitive to wall conductance, increasing with increasing k. A large $\dot{Q}_{min}$ is also undesirable in gas-controlled heat pipes in that it decreases the variable conductance ratio.

---

*The known chemical incompatibility of aluminum and methanol was not of concern in this study.

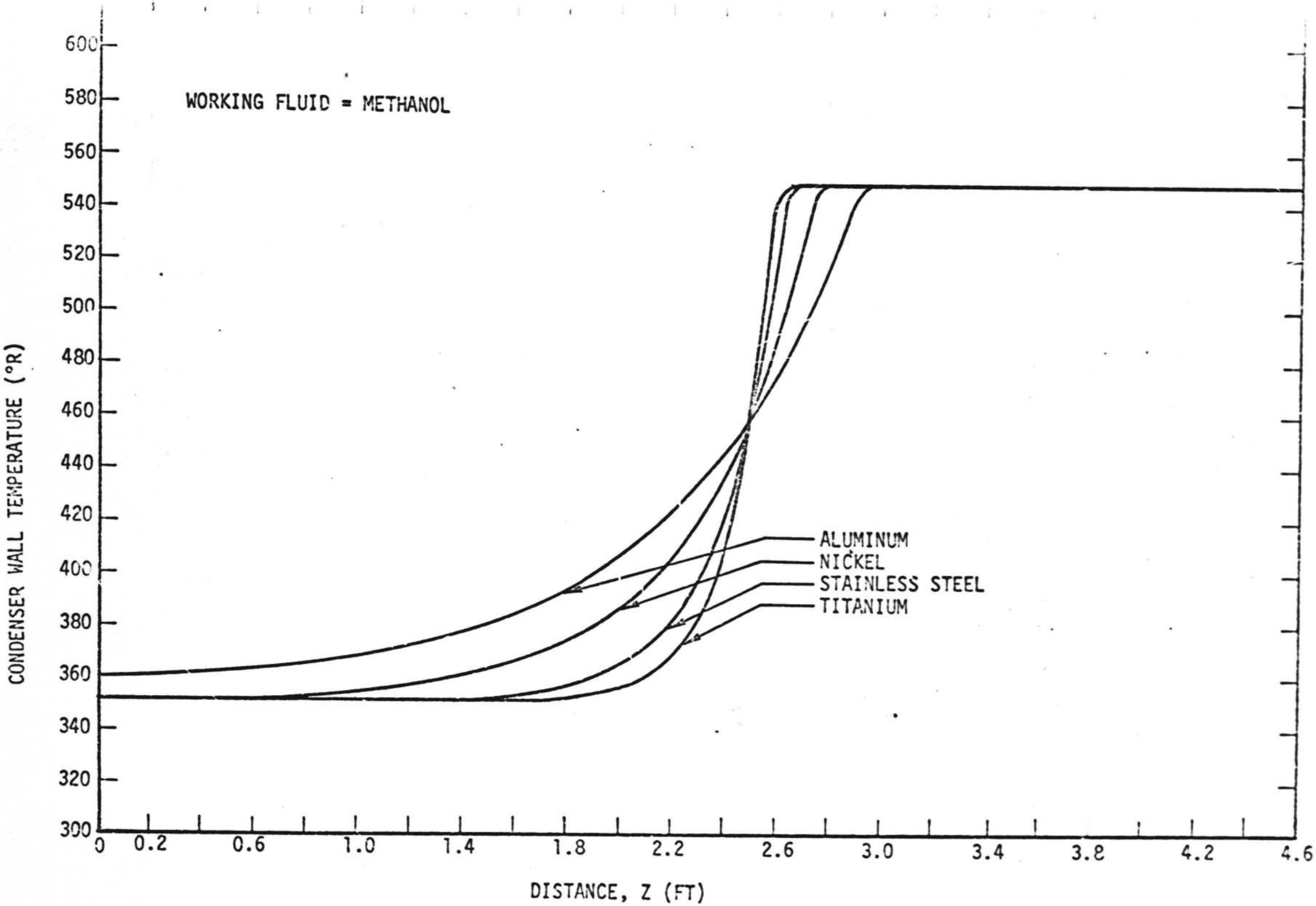

FIGURE 1. Effect of Axial Wall Conductance

TABLE III

Results of Calculations: Diffusion Freezeout Rate, Minimum Power and Total Power

Run	Freezeout Rate (cc/hr)	Minimum Power (Btu/hr)	Total Power (Btu/hr)
Effect of wall material:	Methanol		
1 (titanium)	-	1.9	34.1
2 (stainless)	-	2.5	34.2
3 (nickel)	-	4.2	34.5
4 (aluminum)	-	7.1	35.0
Effect of wall material:	Ammonia		
5 (titanium)	10.0×10^{-4}	2.1	36.7
6 (stainless)	6.7×10^{-4}	2.7	36.5
7 (nickel)	3.6×10^{-4}	4.7	35.9
8 (aluminum)	2.0×10^{-4}	7.9	35.2
Effect of fluid:			
2 (methanol)	-	2.5	34.2
9 (ammonia)	3.0×10^{-5}	2.5	34.1
10 (water)	6.4×10^{-2}	2.8	34.6
Effect of operating temp.:	Ammonia		
6 (550°R)	6.7×10^{-4}	2.7	36.5
11 (500°R)	1.6×10^{-3}	2.1	24.2
12 (450°R)	5.0×10^{-3}	1.6	14.9
Effect of operating temp.:	Methanol		
13 (550°R)	9.0×10^{-7}	2.7	36.5
14 (500°R)	4.1×10^{-6}	2.0	24.3
15 (450°R)	2.8×10^{-5}	1.4	15.0

The computer program also yields the axial mass transport at any position along the condenser. This quantity at the position where the wick reaches the freezing point of the fluid yields the rate at which diffusing vapor freezes and is lost to the system. This "diffusion freezeout rate" is also tabulated in Table III. There are no results shown for the runs corresponding to Fig. 6 because the sink temperature (350°R) was above the freezing point of methanol (322.7°R). However, the ammonia results with a sink temperature below the freezing point show that the freezeout rate increases with decreasing conductivity. This behavior is not surprising in that one expects the diffusion rate to vary with the temperature gradient. Sharp fronts represent high temperature gradients and thus high diffusion rates. Thus, one must examine the magnitude of the diffusion freezeout rate in a given application and, if of consequence, trade this off against the advantages of sharp fronts (lower $\dot{Q}_{min}$, better temperature control) in establishing the axial conductance.

Effect of Working Fluid:

The effect of working fluid is shown on Fig. 7 for water, methanol and ammonia in a stainless steel heat pipe. The results are quite significant. One sees that the profiles are very similar, indicating a relative lack of fluid influence. Such behavior suggests that heat transport by mass diffusion is minimal and axial conduction dominates. This observation is substantiated by the minimum power predictions, which are also nearly equal for the three fluids (Table III).

Although axial mass diffusion does not appear to significantly effect the wall temperature profile, it is both finite and important, for it is the mechanism behind the diffusion freezeout phenomenon. In this regard, Table III indicates substantially different values of predicted diffusion freezeout rates for the three fluids. This variance is due

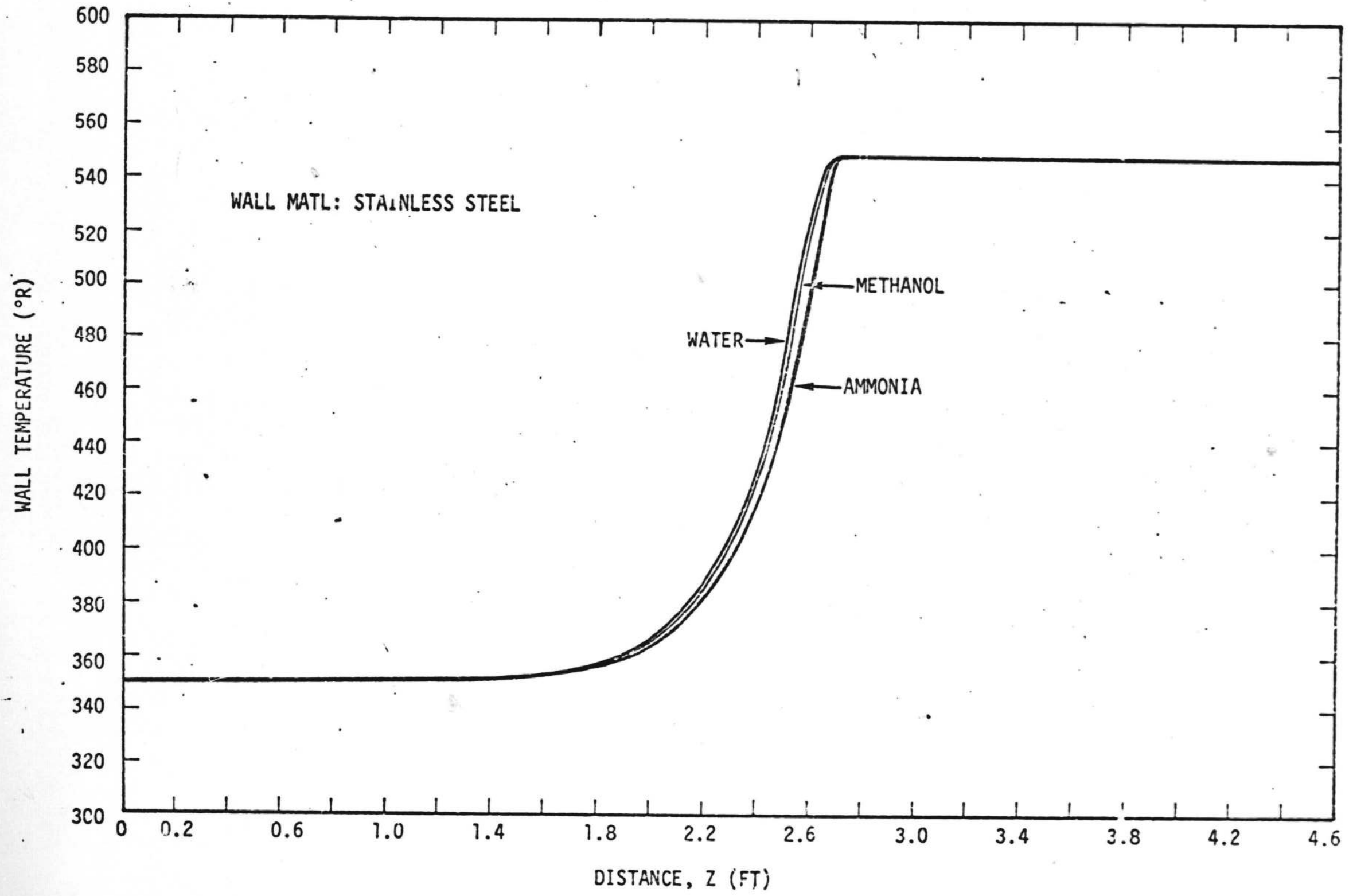

FIGURE 7. Effect of Working Fluid

to a combination of factors including differences in vapor-gas diffusivity, total pipe pressure, and freezing point. Thus, in situations where diffusion freezeout is of potential concern, the choice of working fluid can be of principal importance.

Effect of Operating Temperature:

The primary influence of operating temperature (evaporator temperature) is to alter the pressure in the system. Thus, in view of the previous discussion, one would expect similar temperature profiles as T_{ev} is varied. This is clearly seen in Fig. 8 for ammonia. Varying the operating temperature from 450°R to 550°R has little effect on the shape of the profile. In each case the curves exhibit the characteristic conduction-dominated shape.

Although the effect of pressure on axial diffusion is not reflected in the conduction dominated temperature profiles, it is obvious when one examines the predicted diffusion freezeout rates. Table III shows that for both methanol and ammonia, the diffusion freezeout rate increases as the operating temperature and, hence, total pressure is lowered.

Summary and Conclusions

A study was performed on the heat and mass transfer characteristics of heat pipes containing non-condensible gases. An analysis was formulated based on a one-dimensional model which included (1) simultaneous radiation and convection from a finned condenser, (2) axial conduction in the walls, fins and wicks, (3) binary mass diffusion between the vapor and gas, and (4) an approximate treatment of wick resistance which is accurate for high conductance wicks. The governing equations were programed for numerical solution on a digital computer such that the program can be used for heat pipe design or performance prediction calculations.

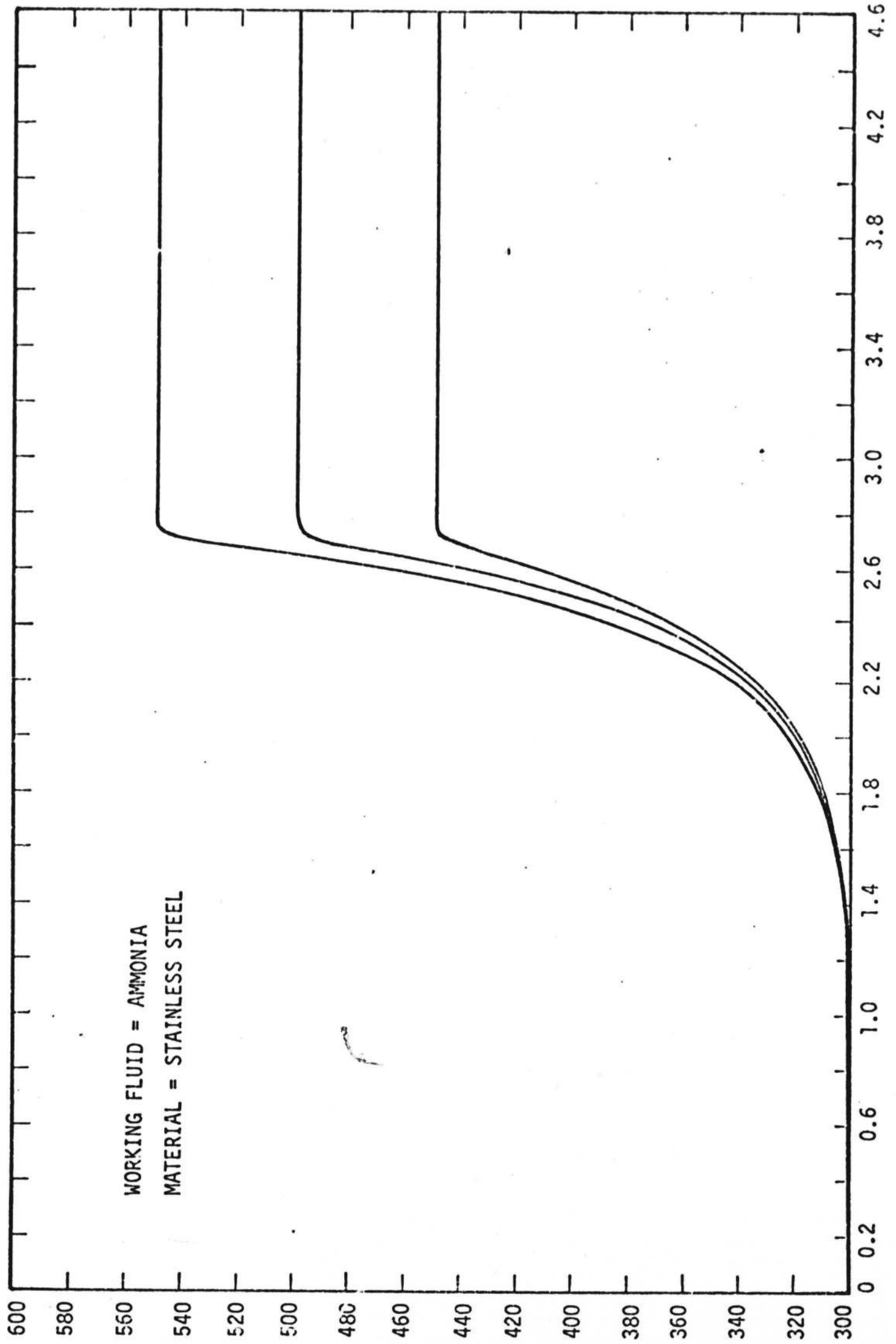

FIGURE 8. Effect of Operating Temperature

Parametric calculations showed an important influence of axial conductance upon the behavior of gas loaded heat pipes. In fact, over the range of variables considered, axial diffusion had negligible impact on the shape of the wall temperature profiles compared with the conduction effect. Thus, the choice of working fluid had little effect on the temperature profiles. Axial diffusion is, however, important in establishing the diffusion freezeout rate for conditions under which this occurs. The freezeout rate varies widely with working fluid and, for a given fluid, increases with decreasing operating temperature (total pressure).

Experimental measurements made with a laboratory heat pipe were in excellent agreement with calculated performance. In particular, the temperature profiles along the pipe wall and the operating characteristic for the pipe (heat rejection vs. evaporator temperature) were correctly predicted.

The experimental verification of the analysis and associated computer program suggests that these may be useful tools for designing gas loaded heat pipes.

APPENDIX

DIMENSIONLESS GOVERNING EQUATIONS

The mass flow rate, mass diffusivity, temperatures, and other parameters were made dimensionless so that orders of magnitudes could be assessed and for convenient numerical solution. The dimensionless quantities are

$$z^* = z/D_e$$

$$V^* = \dot{m}h_{fg}/\dot{Q}_{nominal}$$

$$\mathscr{D}^* = M(c_{ev}\mathscr{D}_{ev}/D_e)A_c h_{fg}/\dot{Q}_{nominal}$$

$$T_i^* = T_i/T_{ev}$$

$$T_w^* = T_w/T_{ev}$$

$$T_0^* = T_0/T_{ev}$$

$$T_c^* = T_c/T_{ev}$$

$$Q_e^* = \frac{d\dot{Q}^*}{dz^*} = S^*(T_w^*-T_c^*)$$

$$S^* = F^*(4\varepsilon\sigma T_i^{*3} + H^*)$$

$$F^* = nPD_e\sigma T_{ev}^4/\dot{Q}_{nominal}$$

$$H^* = h/\sigma T_{ev}^3$$

$$C^* = CT_{ev}/D_e\dot{Q}_{nominal}$$

where T_{ev} is the evaporator temperature which sets the total pressure in the system, and D_e is an equivalent diameter allowing for the presence of arteries within the pipe,

$$D_e = (4A_c/\pi)^{\frac{1}{2}} ,$$

where A_c is the cross-sectional area available for vapor flow. An exponent E is an empirical factor to account for the temperature variation of the mass diffusivity defined by

$$c\mathscr{D} = c_{ev}\mathscr{D}_{ev}(T_i/T_{ev})^E$$

Equations (6), (11), (12), and (8) written in dimensionless form become

$$C^* \frac{d^2T_w^*}{dz^{*2}} + K^*(T_i^* - T_w^*) - S^*(T_w^* - T_c^*) = 0 \quad . \qquad \text{(A-1)}$$

$$\frac{d\phi}{dz^*} = \frac{V^*}{\mathscr{D}^* T_i^{*E}} \qquad \text{(A-2)}$$

$$\frac{dV^*}{dz^*} = K^*(T_i^* - T_w^*) \qquad \text{(A-3)}$$

$$1 - e^{-\phi} = e^{-T_0^*(1/T_i^*-1)} \qquad \text{(A-4)}$$

Under approximation 2 in the list in the text, Eq. (A-1) is approximated as

$$C^* \frac{d^2T_i^*}{dz^{*2}} + K^*(T_i^*-T_w^*) - S^*(T_w^*-T_c^*) = 0 \qquad \text{(A-1a)}$$

The simplifying feature of this approximation is that the second derivative in Eq. (A-1a) can now be eliminated. Equation (A-4) is differentiated with respect to z^*, and Eq. (A-2) is used to eliminate $d\phi/dz^*$. The result multiplied by C^* is

$$C^* \frac{dT_i^*}{dz^*} = C^* \frac{e^{-\phi}}{1-e^{-\phi}} \frac{T_i^{*2-E}}{\mathscr{D}^* T_0^*} V^* \qquad \text{(A-5)}$$

Equation (A-5) is differentiated again with respect to z^*, Eq. (A-2) is used again to eliminate $d\phi/dz^*$, and Eq. (A-5) itself is used to eliminate dT_i^*/dz^*.

$$C^* \frac{d^2T_i^*}{dz^{*2}} = \Phi_1 \frac{dV^*}{dz^*} - \Phi_1 \zeta_2 \Phi_3 \tag{A-6}$$

where the functions Φ_1, Φ_2, Φ_3 are

$$\Phi_1(\phi) = C^* \frac{e^{-\phi}}{(1-e^{-\phi})} \frac{T_i^{*2-E}}{\mathscr{P}^* T_0^*} \tag{A-7}$$

$$\Phi_2(\phi) = 1 - (2-E)(T_i^*/T_0^*)e^{-\phi} \tag{A-8}$$

$$\Phi_3(\phi, V^*) = V^{*2}/ (1-e^{-\phi})\mathscr{P}^* T_i^{*E} \tag{A-9}$$

Equation (A-1a) together with Eqs. (A-3) and (A-6) now can be written

$$\frac{dV^*}{dz^*} = Q_e^* - \Phi_1 \Phi_4 \tag{A-10}$$

where

$$\Phi_4(\phi, V^*) = \frac{Q_e^*(\phi) - \Phi_2(\phi)\Phi_3(\phi, V^*)}{1 + \Phi_1(\phi)} \tag{A-11}$$

Equations (A-2) and (A-10) together with (A-4) and the definitions of Φ_j in Eqs. (A-7, A-8, A-9, and A-11) form a set of two simultaneous nonlinear first order ordinary differential equations which can be numerically solved by, say, a fourth-order Runge-Kutta routine. The initial conditions are $V^* = 0$ and $\phi = \phi_0$ at $z = 0$. Values of $\mathscr{m}$ and $\dot{Q}$ for a length of pipe L can be obtained versus ϕ_0 for a given set of parameters and an evaporator temperature T_{ev}. An iterative routine can be used to find ϕ_0 for a prescribed value of either $\mathscr{m}$ or $\dot{Q}$.

Acknowledgments

The authors with to express their appreciation to Mr. George Fleischman of TRW for his efforts in both the experimental and computational phases of this work.

This paper is based on work performed under NASA Ames Research Center Contract NAS 2-5503. Mr. J. P. Kirkpatrick serves as NASA Project Manager for this contract.

References

1. B. D. Marcus and G. L. Fleischman, "Steady-State and Transient Performance of Hot Reservoir Gas-Controlled Heat Pipes", A.S.M.E. Paper No. 70-HT/SpT-11.

2. W. Bienert, "Heat Pipes for Temperature Control", Proceedings: Fourth Intersociety Energy Conversion Engineering Conference, Washington, D. C., September 1969.

3. J. D. Hinderman, J. Madsen and E. D. Waters, "An ATS-E Solar Cell Space Radiator Utilizing Heat Pipes", AIAA Paper No. 69-630, AIAA 4th Thermophysics Conference, San Francisco, Calif., June 1969.

4. J. E. Deverall, "Mercury as a Heat Pipe Fluid", A.S.M.E. Paper No. 70-HT/SpT-8.

5. O. W. Clausen, B. D. Marcus, W. E. Piske and R. C. Turner, "Circumferential Heat Pipe Systems for Large Structures", Final Report - NASA Contract No. NAS 9-10299, December 1970.

Nomenclature

A_c	-	Cross sectional area
C	-	Axial conductivity-area product
D	-	Diameter
$\mathscr{D}$	-	Diffusion coefficient for non-condensible in condensible
E	-	Empirical constant for temperature dependence of
F*	-	Non-dimensional quantity defined in Appendix
H	-	Irradiation onto condenser surface
K	-	Radial wick conductance
L	-	Length of condenser
M	-	Molecular weight of condensible
$\mathscr{m}$	-	Molar inventory of non-condensible
P	-	Heat transfer perimeter of fin
P_i	-	Partial pressure of non-condensible at temperature T_i
$\dot{Q}$	-	Heat transfer rate
Q_e^*	-	Non-dimensional quantity defined in Appendix
R	-	Gas constant for condensible
R_u	-	Universal gas constant
S	-	Radial conductance from condenser
T	-	Temperature
T_o	-	Characteristic temperature of fluid defined by Eq. (8b)
V	-	Mole average velocity
c	-	Molar concentration
h	-	Coefficient of heat transfer
h_{fg}	-	Latent heat of vaporization
k	-	Thermal conductivity
$\dot{m}$	-	Mass flow rate
q	-	Heat flux
x	-	Mole fraction
z	-	Axial position

α - Absorptance of condenser surface

δ - Wick thickness

ε - Total hemispherical emittance of condenser surface

ϕ - Dimensional variable defined by Eq. (10)

Φ_1, Φ_2, Φ_3, Φ_4 - Dimensionless groups defined in Appendix

η - Effectiveness of condenser fin

σ - Stefan-Boltzmann constant

Subscripts:

abs - Absorbed from surrounds

b - Bulk average (area-velocity weighted) value

c - Effective sink conditions

e - Equivalent value

ev - Evaporator conditions

f - External fluid conditions

i - Wick surface conditions

min - Minimum

nominal - Initialized value for numerical solution

n - Cross-sectional element of pipe

s - Spatial (area weighted) average

w - Condenser wall conditions

* - Superscript denotes non-dimensional variable